Interfacing Polymers and Tissues: Quantitative Local Assessment of the Foreign Body Reaction of Mononuclear Phagocytes to Polymeric Materials

Elena Giusto, Matteo Donegà, Andra C. Dumitru, Giulia Foschi, Stefano Casalini, Michele Bianchi, Tommaso Leonardi, Alessandro Russo, Luigi G. Occhipinti, Fabio Biscarini, Ricardo Garcia,* and Stefano Pluchino**

A quantitative method to assess the in vitro foreign body reaction (FBR) of mononuclear phagocytes (MP) to polymers relevant in implants for prosthetics, advanced therapies, and regenerative medicine is presented. It integrates single-cell force spectroscopy (SCFS) with immunogenic profiles of the MPs. In cell force spectroscopy experiments a single phagocyte, linked at the end of an atomic force microscopy cantilever, probes the adhesion forces between the cell and the polymer surface. SCFS measures adhesion forces in a range from 10 pN to 100 nN and with spatial resolution from cell size down to nanometers, accessing the early adhesion events established at contact times between milliseconds and minutes. The time evolution within the first 60 s of the adhesion force between the phagocyte and the polymer surface before and after the treatment with an immunosuppressive drug, viz. Minocycline, a Federal Drug Administration (FDA)-approved third generation tetracycline with anti-inflammatory effects, is then studied. The adhesion force values measured at the single cell level is shown to correlate to the immunogenic profiles obtained by analysis of biomarkers and morphology of the MPs in culture. Also, Minocycline causes a decrease of both proinflammatory gene expression profiles and adhesive forces of single cells.

1. Introduction

Synthetic biomaterials are widely used to fabricate medical devices regulating, replacing, or restoring impaired functions of the body. These applications are expected to grow with the advent of advanced therapies based on loco-regional treatments or stem-cell grafts for tissue regeneration.[1,2]

The implantation of any material or medical device into a host tissue is likely to trigger an adverse foreign body reaction (FBR),[3] which is a cascade of events strongly intertwined with the interactions between cells and materials. FBR starts with recruitment, adhesion and accumulation of white blood cells (*leukocytes*)—including neutrophils and monocytes/macrophages—at the tissue-implant interface.[2] Upon adhesion, activated mononuclear phagocytes (MPs) fuse into giant cells in the attempt of engulfing the

Dr. E. Giusto, Dr. M. Donegà, Dr. T. Leonardi, Dr. S. Pluchino
Department of Clinical Neurosciences
Wellcome Trust–Medical Research Council Stem Cell Institute and National Institute for Health Research Biomedical Research Centre
University of Cambridge
Hills Road, Cambridge CB2 0HA, UK
E-mail: spp24@cam.ac.uk

Dr. A. C. Dumitru, Prof. R. Garcia
Instituto de Ciencia de Materiales de Madrid, CSIC
Sor Juana Inés de la Cruz 3, 28049 Madrid, Spain
E-mail: r.garcia@csic.es

Dr. G. Foschi,[+] Dr. S. Casalini,[++] Prof. F. Biscarini
Dipartimento di Scienze della Vita
Università di Modena and Reggio Emilia
Via Campi 103, 41125 Modena, Italy
E-mail: fabio.biscarini@unimore.it

Dr. M. Bianchi, Dr. A. Russo
Laboratorio di NanoBiotecnologie-Istituto Ortopedico Rizzoli
Via di Barbiano 1/10, 40136 Bologna, Italy

Dr. T. Leonardi
The EMBL-European Bioinformatics Institute
Wellcome Trust Genome Campus
Hinxton, Cambridge CB10 1SD, UK

Dr. L. G. Occhipinti[+++]
STMicroelectronics Srl
Stradale Primosole 50, 95121 Catania, Italy

[+]Present address: Scriba Nanotecnologie S.r.l., Via di Corticella 183/8, 40128 Bologna, Italy.

[++]Present address: Institut de Ciència de Materials de Barcelona (ICMAB), Consejo Superior de Investigaciones Cientificas (CSIC), Universitat Autònoma de Barcelona (UAB campus), 08193 Bellaterra, Barcelona, Spain.

[+++]Present address: Department of Engineering, Electrical Engineering Division, University of Cambridge, 9 JJ Thomson Avenue, Cambridge CB3 0FA, UK.

DOI: 10.1002/adbi.201700021

foreign body. Activated MPs release a plethora of proinflammatory signals such as cytokines, chemokines, reactive oxygen intermediates, nitric oxide, and degrading enzymes to finally recruit additional immune cells and fibroblasts.[2] In later chronic phases, fibroblasts and mast cells produce a collagen-based extracellular matrix that wraps the implanted material/device into a fibrotic, avascular capsule, thus preventing any interaction with the surrounding tissue and impairing the long-term functionality of the implant.[4,5]

The origin of FBR is not completely understood. Correlations have been assessed between bulk and surface materials properties, such as elasticity and plasticity, surface morphology and texture, wettability and surface tension, and the initial adhesion of cells to substrates.[6–10] Because cell/material adhesion is a multiscale phenomenon, there is a lag in accessing the cell/material interaction from the single cell down to the molecular level.

Most of the studies focusing on FBR are based on phenomenological or semiquantitative cell adhesion assays in vitro.[10] The established methodologies foresee the detection of relevant biomarkers expressed by cells of the immune system, together with the evaluation of cell morphological parameters. In vitro assays imply a lengthy response, large variances of the observables, and difficult standardization of the protocols. Advancing the methodology from the heuristic level to a robust quantitative characterization in a shorter timescale is important both for materials screening, as well as to evaluate the synergic effects of drugs and chemotrophic factors that may prevent or delay the onset of cell adhesion.

Here, we present a quantitative method to assess the in vitro FBR of MPs to polymers relevant in implants for prosthetics, advanced therapies, and regenerative medicine. Our approach integrates single-cell force spectroscopy (SCFS) with immunogenic profiles of the MPs. In the cell force spectroscopy experiments a single phagocyte, linked at the end of an AFM cantilever, probes the adhesion forces between the cell and the polymer surface. SCFS measures adhesion forces in a range from 10 pN to 100 nN and with spatial resolution from the cell size down to nanometers,[11] and accesses the early adhesion events established at contact times between milliseconds and minutes.[12–14] We study the time evolution (1–60 s) of the adhesion force between the phagocyte and the polymer surface before and after the treatment with an immunosuppressive drug. Specifically, we use Minocycline, a Federal Drug Administration (FDA)-approved third generation tetracycline with anti-inflammatory effects. We find that the adhesion force values measured at the single cell level correlate to the immunogenic profiles obtained by analysis of biomarkers and morphology of the MPs in culture, and that Minocycline causes a decrease of both proinflammatory gene expression profile and adhesive force of single cell.

2. Results and Discussion

We choose poly-dimethylsiloxane (PDMS)—a biocompatible non-biodegradable polymer—and poly-(lactic-*co*-glycolic acid) (PLGA)—a biocompatible and biodegradable polymer—as prototypical polymeric materials for biomedical applications.[15,16]

Table 1. Morphological parameters and mechanical properties of the polymer substrates investigated.

Polymer substrate	rms roughness [nm]	Reduced Young's modulus E_r [GPa]	Hardness H_c [MPa]
PDMS	2.5 ± 1.0	0.10 ± 0.02	10 ± 1
PLGA	0.5 ± 0.2	6.5 ± 0.3	175 ± 20
PS	3.0 ± 0.5	5.5 ± 0.5	245 ± 20

They are cast as films with 100 μm (PDMS) and 5 μm (PLGA) thickness. Cells are usually seeded on polystyrene (PS) petridishes, hence this material is used as the control interface for mechanical and topographical properties. In addition, Lypopolysaccharide (LPS) is used as positive proinflammatory stimulator. Our specific interest on PDMS and PLGA arises from their potential use as scaffolds for organic electronic implants, whose operation timescale is tailored to a few months, for the advanced treatment of pathologies of the nervous system as for instance spinal cord injury. The thickness values chosen for the different materials are relevant to the devices that we plan to implant in animal model.

The morphological parameters and mechanical properties measured on the PS, PLGA, and PDMS surfaces are reported in **Table 1**. All surfaces exhibit a smooth featureless morphology with a (saturated) root-mean-square (rms) roughness <5 nm (*AFM images not shown*). The mechanical properties of PS, PLGA, and PDMS are measured by nanoindentation. The reduced elastic modulus E_r is below 100 MPa for PDMS, more than ten times softer than PS (5 GPa) and PLGA (6.5 GPa). PDMS exhibits a low contact hardness H_c value (5 MPa) compared to PLGA (150 MPa) and PS (about 250 MPa).

To evaluate the medium-term interaction of MPs with substrates, we quantify the number density and the morphology of adhering cells from fluorescence images. MPs exhibit different morphologies: small and rounded when plated on PDMS, large and spread when plated on PLGA and PS (with or without addition of LPS) (**Figure 1**a). Significant differences are observed in the number of cells per unit area adhering to the materials, with PDMS showing the lowest and PLGA the highest numbers of adhering MPs both after 1 h (Figure 1b) and 24 h in vitro (Figure 1c). As the fraction of cells at 24 h with respect to those at 1 h increased only by a few to few tens percent (over total plated) on all of the materials tested, we infer that the above difference depends on the different adhesive response of MPs, and not on the proliferation rates, consistently with previous observations on organic thin films.[17]

The MPs morphology is quantified by extracting the average projected area of the cells (Figure 1d) and their elongation factor (Figure 1e), a parameter that has been previously associated with the functional state of MPs.[18] Cell adhesion and migration are also accompanied by the formation of filopodia, thin spike-like cytoplasmic outgrowth containing bundles of parallel actin filaments that act as *fingers* probing the microenvironment in adhering/migrating cells.[19] PLGA promotes extensive formation of filopodia, while PDMS shows an opposite effect leading to smooth cell contours (Figure 1f). Complete morphological analysis at 1h (e.g., including elongation factor, cell area, and filopodia

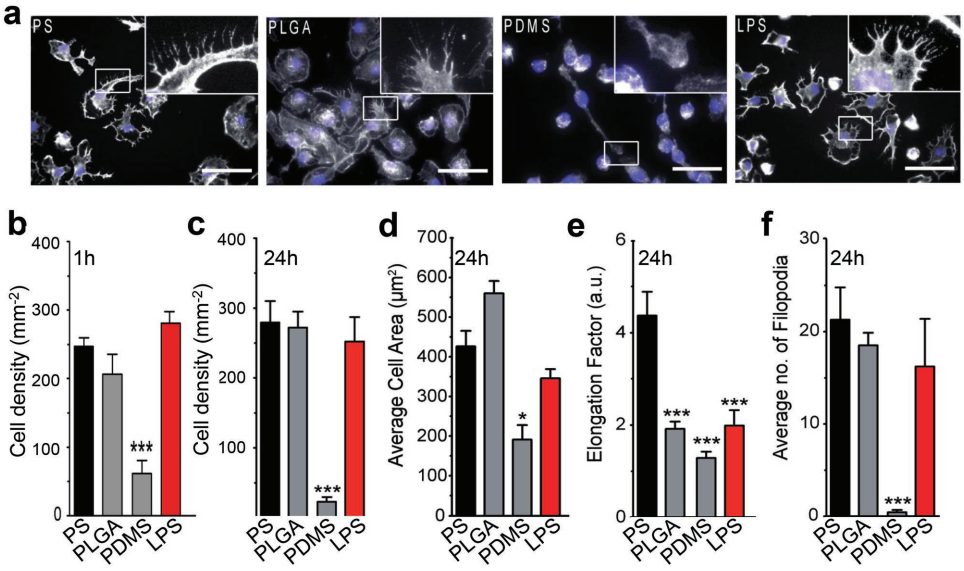

Figure 1. a) Fluorescence images of MPs adhering to PS and polymer films in vitro 24 h after plating. Insets evidence the development of filopodia. Cytoskeleton is labeled with Phalloidin (gray) and nuclei are labeled with DAPI (blue). Scale bar is 50 μm; b–f) quantification of morphological features of MPs adhered to different substrates: cell density at b) 1 h and c) 24 h, d) cell area at 24 h, e) elongation factor at 24 h, f) and number of filopodia at 24 h. Lipopolysaccharide (LPS)-activated MPs were used as positive controls (right image of (a) and red bars in (b–f)). Data are expressed as mean value ± SEM and analyzed with One-Way-Anova and Bonferroni's post-test correction. $*p \leq 0.05$; $**p \leq 0.005$; $***p \leq 0.001$, versus PS.

formation) cannot be provided since cell adhesion is not conclusive at this early time point.

We then assess the activation of MPs by profiling the expression level of the pro-inflammatory genes Tumor necrosis factor-α (*Tnf-α*), Interleukin 1β (*Il1b*), *Il6,* and Nitric oxide synthase (*Nos2)* as well as of the anti-inflammatory genes Arginase 1 (*Arg1)* and Mannose Receptor I (*MrcI)* at 6 and 24 h after plating in vitro. These are classical markers for proinflammatory (M1) and anti-inflammatory (M2) macrophages.[20,21] The results are shown in **Figure 2**a–f. PLGA shows a prolonged proinflammatory activation of MPs lasting until 24 h, whereas PDMS shows a similar profile at 6 h, which is then reduced at 24 h leading to the lowest proinflammatory response of MPs, when compared to PS.

Unsupervised clustering of material properties and their FBR profile reveals a correlation between MP adhesion and the material's elastic modulus and hardness (Figure 2g). On the other hand, MP activation as measured by cytokine expression is mostly influenced by the presence of LPS, whereas the different materials have a more modest contribution. These observations are in line with the notion that MPs behavior is regulated by soluble factors as well as by the chemical-physical properties of the environment, and suggest that whereas activation by LPS drives cytokine secretion, the chemical–physical properties of the material have greater impact on the morphological features of activated MPs.

To elucidate the interactions occurring between MPs and polymer films we perform SCFS measurements in a serum-free setting. In our approach the cantilever is amino-functionalized and coated with fetal bovine serum. Then a single MP is linked to the end of the cantilever, with the aim of measuring the force as a function of the probe-surface distance (force curve). The analysis of force curves recorded while detaching a single MP from the substrate suggests a complex interaction characterized by (1) a sharp increase of the adhesion force corresponding to the elastic stretching of the entire cell; (2) a sequence of de-adhesion steps attributed to the unbinding of cell membrane proteins from the surface; (3) a region of plateaus of constant force extending around 1000 nm distance due to the detachment from the surface of micrometer-long membrane tethers; (4) a complete detachment of the cell from the surface (**Figure 3**a,b).

To compare the strength of adhesion on PLGA (Figure 3a) and PDMS (Figure 3b), we measure the adhesion forces of MPs for contact times of 10 and 30 s (Figure 3c). The data include 20 cells and each measurement involves the acquisition and average of 10 force curves per each contact time. We measure >1.5-fold higher adhesion forces on PLGA (492 ± 118 pN at 10 s and 805 ± 269 pN at 30 s) than PDMS (306 ± 73. pN at 10 s and 409 ± 121 pN at 30 s), which increases upon longer contact time only on PLGA. We also observe a larger standard deviation on PLGA than on PDMS. The variation coefficients (ratio of standard deviation to mean) on PDMS and PLGA are comparable (0.23 at 10 s, 0.3 at 30 s). This indicates that the force curves measured between MPs and PDMS result from similar interactions and the greater mean and dispersion in the case of PLGA arise from an increasing number of the adhesion proteins in the extracellular membrane expressed by the MP interacting with PLGA.

Based on the above observations, and the relevance of PLGA for the fabrication of bioresorbable implants, we test the effects of Minocycline on the adhesion and activation of MPs on PLGA. MPs are plated on PLGA and treated for 24 h with two different doses (10×10^{-6} and 50×10^{-6} M) of Minocycline. As

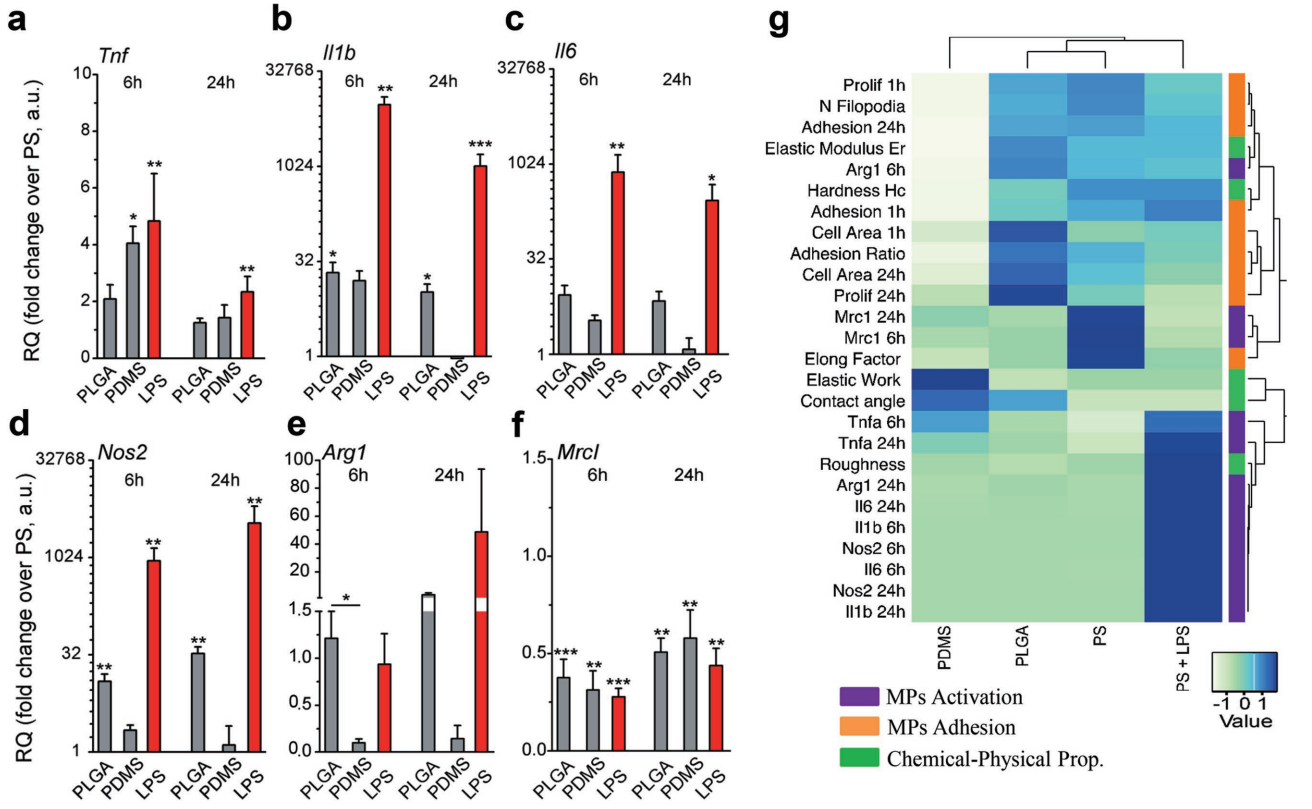

Figure 2. Analysis of inflammatory biomarkers expressed by MPs on PDMS and PLGA, and PS: qRT-PCR analyses showing changes in the expression of a) *Tnf*, b) *Il1b*, c) *Il6*, and d) *Nos2 (*proinflammatory) and e) *Arg1* and f) *Mrcl* (anti-inflammatory) mRNAs in MPs at 6 and 24 h in vitro. PS ± LPS were positive and negative controls (black and red bars, respectively). Data were obtained from $n \geq 3$ independent experiments, and expressed as mean fold change (over PS) ± SEM. Data were analyzed with one-way-Anova and Bonferroni's post-test correction. LPS, lipopolysaccharide; RQ, relative quantity. $*p \leq 0.05$; $**p \leq 0.005$; $***p \leq 0.001$, versus PS. g) Heatmap summarizing the immunogenic properties (as in panels a–f) and chemical–physical properties (as in Table 1 and Figure 1b–f) of PDMS, PLGA, and PS with and without LPS. The color scale represents scaled values (see the Experimental Section).

shown in **Figure 4**a,b, 50×10^{-6} M Minocycline is effective in reducing the formation of filopodia of MPs seeded on PLGA. Minocycline-treated MPs are also analyzed by means of SCFS at increasing contact times of 5, 10, 30, and 60 s on PLGA. The data set includes $n \geq 15$ cells and $n \geq 3$ force curves per contact time. Figure 4c shows the adhesion force as a function of the contact time for untreated and Minocycline-treated cells. The mean value of the adhesion force at 5 s seems not to be influenced by the Minocycline treatment. However, significant differences are recorded for longer contact times. The adhesion force of untreated cells shows a threefold increase with time (527 ± 174 pN at 5 s and 1469 ± 502 pN at 60 s), while the mean value of Minocycline-treated cells remains almost constant in the 5–30 s range (486 ± 101 pN at 5 s and 578 ± 204 at 30 s) with an increase at 60 s (754 ± 360 pN) which is not statistically significant.

These results suggest that the decreased adhesion force between MPs and PLGA is correlated to the administration of Minocycline. Importantly, Minocycline does not affect MP viability at any concentration tested (*data not shown*). Minocycline (both 10×10^{-6} and 50×10^{-6} M) is also able to reduce MP activation, as shown by the downregulation of *Tnf, Il1b, Il6,* and *Nos2* at any concentration tested (**Figure 5**). We cannot make any hypotheses on how Minocycline intervenes on cell adhesion at this stage. The finer mechanism behind the action of Minocycline is not accessible to our comparative experiment, and further studies are indeed required. The outcome is that, albeit PLGA is clearly immunogenic, the FBR of the monocytes against PLGA can be reduced by the local supply of Minocycline.

3. Conclusions

In conclusion, we demonstrate the existence of a correlation between the adhesion force of MPs to synthetic polymer surfaces and their activation toward FBR in vitro. In particular, the large mean value and spread of the adhesion force is correlated to the proinflammatory response of the MPs. The action of an anti-inflammatory drug such as Minocycline on the MPs yields a measurable decrease of their adhesive force, and hence inhibits the FBR induced by PLGA. Our evidence indicates that adhesion is a potential target to minimize the FBR against materials that are immunogenic a priori.

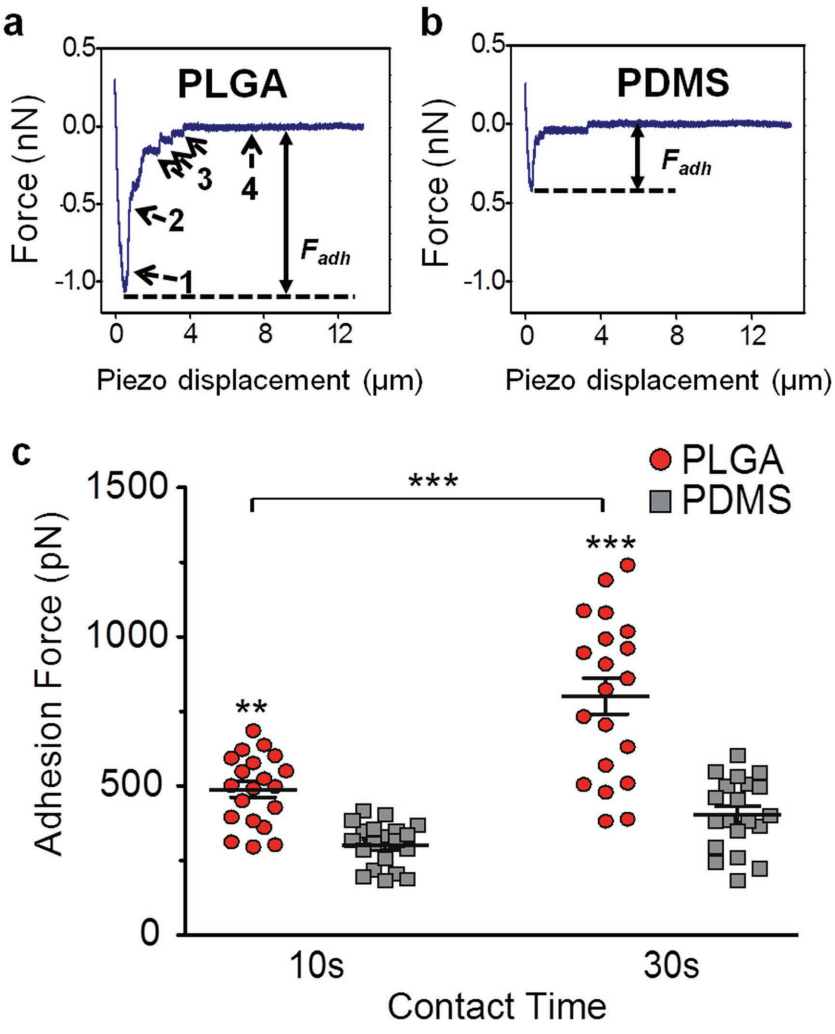

Figure 3. Typical force curve (retraction or unloading part) from representative SCFS experiments on a) PLGA and b) PDMS. Key features are marked: (1) increase of the adhesion force corresponding to the elastic stretching of the entire cell, (2) deadhesion steps, which can attributed to the unbinding of cell membrane proteins, (3) plateaus of constant force due to the detachment from the surface of micrometer-long membrane tethers, and (4) detachment of the cell from the polymer surface. c) Quantification of adhesion force (pN) on PLGA (red dots) and PDMS (gray squares) samples, at two different contact times (10 and 30 s). At least 15 cells were tested in alternating measurements for each material. Data are expressed as mean values ± SEM and analyzed with One-Way-Anova and Bonferroni's post-test correction.

SCFS provides a faster (on the seconds to minutes timescale) indication than the morphological analysis and biomarkers profile (on the 24 h timescale) on the affinity between cells of the immune system and the materials surface. Cell adhesion strength can be quantified by means of SCFS with high sensitivity and the adhesion dynamics monitored in real time. In SCFS there is no need for fluorescent labelling of the samples, or to fix the cells, and, furthermore, the data analysis is not as time consuming and operator-dependent as in the case of the simple morphological analysis. SCFS could become an effective tool to screen the immunogenic potential of materials and to assess in vitro the efficacy of chemical or pharmacological treatments.

4. Experimental Section

Preparation of Materials: PLGA (molecular weight: 66 000–107 000) composed by a 75:25 ratio of D,L-lactide and glycolide units was purchased from Sigma-Aldrich (P1941) and used as received. PLGA films were prepared by solution casting method. PLGA was dissolved in dichloromethane upon stirring for about 40 min at room temperature to obtain a 1 wt% solution. A volume of 100 µL of this solution was then cast onto a cleaned glass slide (Thermo Scientific) into a square frame (Sigma, S1815, Secure Slip glass coverslip silicone 1.2 cm × 1.2 cm) to obtain a thin layer of the solution with defined geometry and thickness. The solvent was allowed to evaporate at 55 °C for 5 h in an oven, and then the frame was removed. The resulting transparent film was disinfected in 99% ethanol for 15 min and dried in air before using it. A film thickness of ≈5 µm was measured.

PDMS (Sylgard 184, Dow Corning) was mixed in a 10:1 (w/w) ratio of silicone and curing agent and placed in a vacuum chamber. The PDMS films (100 µm thick) were obtained by spin coating (spin speed 500 rpm, acceleration 500 rpm s^{-1}, and duration time 3 min) and postbaking in an oven at 120 °C for 1 h.

Polystyrene tissue culture-treated 24-well plates (Corning, #07-200-84) were used as controls.

Amplitude Modulation AFM Imaging: The topography of PLGA, PDMS, and PS was measured in air environment with a Nanowizard III AFM (JPK Instruments, Germany) in amplitude modulation AFM by mechanically driving the cantilever.[22] Rectangular PPP-NCH (Nanosensors, Switzerland) cantilevers with a nominal force constant $k = 40$ N m^{-1} and a resonant frequency of 291 kHz were employed in these measurements. Images were then processed with the JPK Data Processing Software and the roughness value was extracted (root-mean square, rms).

Nanoindentation Tests: Mechanical tests were performed in air and at 21 °C using a standard nanoindentation tester (NHT2, CSM Instruments, Peseux, Switzerland) equipped with a Berkovich diamond tip (plain strain modulus: 75.1 ± 0.4 GPa, estimated silica Poisson's ratio: 0.16). The reduced elastic modulus (E_r) and the contact hardness (H_c) were estimated from the load (P) versus depth (h) curve according to the method by Oliver and Pharr.[23] E_r was calculated from the slope of the unloading curve in the region between 40% and 98% of the maximum load according to

$$E_r = \frac{\sqrt{\pi}}{2}\frac{S}{\sqrt{A_c}} \quad (1)$$

where S is the contact stiffness, calculated from the initial slope of the unloading curve (dP/dh), and A_c is the contact area.

H_c was calculated as

$$H_c = \frac{P_{max}}{A_c} \quad (2)$$

where P_{max} is the maximum applied load.

A linear loading (loading and unloading rate set at 1.8 mN min^{-1}) for a maximum load of 0.3 mN was used. Due to the extreme elastic

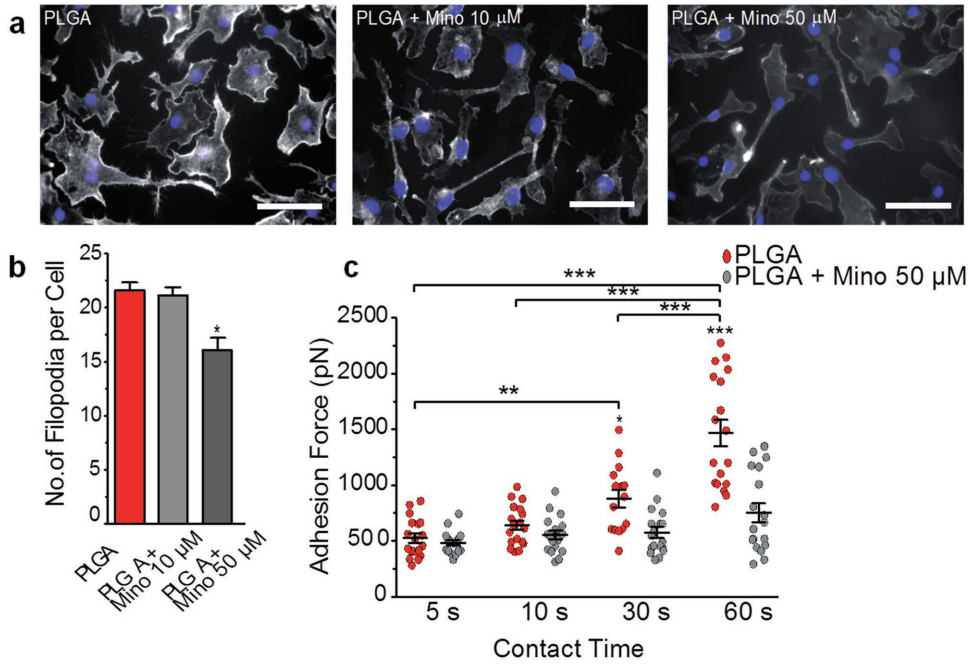

Figure 4. a) Fluorescence images of MPs adhering to PLGA without Minocycline (left), 10×10^{-6} M Minocycline (center), and 50×10^{-6} M Minocycline (right) after 24 h in vitro. Cytoskeleton is labeled with Phalloidin (gray) and nuclei are labeled with DAPI (blue). b) Quantification of filopodia formation 24 h after plating on PLGA and PLGA + Minocycline as in (a). c) SCFS-based quantification of adhesion force to PLGA: control (red) versus Minocycline-treated (gray) MPs at 5, 10, 30, and 60 s after contact. Scale bar in (c): 50 μm. *$p \leq 0.05$; **$p \leq 0.005$; ***$p \leq 0.001$, versus controls.

behavior of PDMS, a linear loading (loading and unloading rate set at 120 mN min^{-1}) for a maximum load of 20 mN was required. The maximum loads were chosen in order to achieve a maximum indentation smaller than the 10 % of film thickness, thus to strongly limit the contribution of the mechanical properties of the substrate.[24]

In order to limit the viscoelasticity contribution due to the time dependent behavior of investigated samples, a creep hold of 60 s has been introduced at peak load.[25,26] The control of the thermal drift was automatically performed by the system between each indentation. All the data resulting from explicitly inadequate contact points were discarded

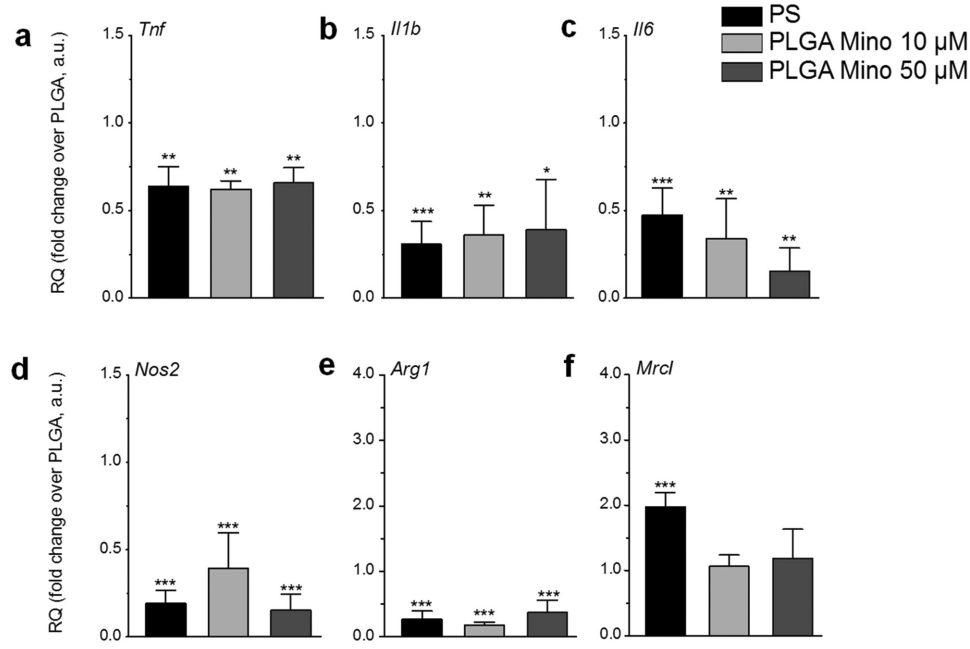

Figure 5. qRT-PCR analyses showing changes in the expression of a) *Tnf*, b) *Il1b*, c) *Il6*, d) *Nos2* (proinflammatory), and e) *Arg1* and f) *Mrcl* (anti-inflammatory) mRNAs in MPs on PLGA after 24 h with Minocycline 10×10^{-6} M (light gray bars) or 50×10^{-6} M (dark gray bars). MPs on PLGA only (black bars) were used as control. Mino, Minocycline; RQ, Relative quantity. *$p \leq 0.05$; **$p \leq 0.005$; ***$p \leq 0.001$, versus PLGA.

from the data set analysis. At least eight indentation measurements were performed on different areas within each sample and the results provided as mean ± SD.

Contact Angle Measurements: The contact angle measurements were performed by a Digidrop GBX Model DS on droplets (0.7 µL) of bi-distilled water placed on the polymer substrates at RT.

SCFS: Cell adhesion measurements were conducted using a Nanowizard III AFM (JPK Instruments, Germany) mounted on top of an inverted optical microscope (Axiovert A1, Zeiss, Germany). To attach a single cell, the cantilever was lowered toward the petri dish at a speed of 5 µm s^{-1} and pressed onto a cell by applying a contact force of 3 nN for 5 s. Then the cantilever was pulled 50 µm away from the sample surface. A resting period of 10 min was introduced before the adhesion measurements. The microcantielver with the cell attached to it was then approached toward the relevant material surface at a speed of 5 µm s^{-1} until reaching a contact force of 0.3–0.5 nN.

All reagents used for the cantilevers functionalization were purchased from Sigma-Aldrich (Spain). Tipless microcantilevers (NPO-10, Bruker, USA) were first cleaned thoroughly by immersion in a solution of 0.25 M sulfuric acid and 9.8 M hydrogen peroxide 4:1 (v/v) for 30 min. The cantilevers were rinsed with ultrapure water and then immersed into a solution of APTES–water–ethanol 5:5:90 (v/v/v) for 30 min. The resulting amino-functionalized microcantilevers were rinsed with ultrapure water, ethanol, dried with nitrogen gas and stored in a dry atmosphere. The microcantilevers were finally immersed in 10% FBS at 4 °C overnight, rinsed ten times in 0.01 M phosphate buffer saline (PBS) (pH 7.4) and stored at 4 °C in a glass Petri dish. The tipless cantilevers (nominal spring constant 0.06 N m^{-1}) were calibrated before starting the cell adhesion measurements. The optical lever sensitivity was calibrated by acquiring deflection versus distance curves on a hard surface (mica). One hundred deflection-versus-distance curves were acquired and the sensitivity of the photodiode was calculated as the mean value of the slope of the deflection curve measured in the repulsive region. The force constant k and quality factor of the cantilevers were determined by using the thermal noise method.[27] The calibrated k was found in the 0.05–0.07 N m^{-1} range. The force was then calculated by using Hooke's law, $F = -k \cdot \Delta z$, where Δz is the cantilever deflection.

Isolation and Differentiation of MPs from the Bone Marrow: All the procedures were performed accordingly to the principles of laboratory animal care approved by the UK Home Office animals (scientific procedures) act 1986. Bone-marrow-derived monocytes were isolated from adult C57BL/6 male mice (Jax).[28]

Briefly, mice were euthanized followed by neck dislocation. Femurs and tibias were collected, cleaned of the muscles and flushed using 25 gauge needles mounted on 10 mL syringes filled with high glucose DMEM medium (Life Technologies, #41966-029). A hypotonic solution (NH4Cl 0.8%, pH 7.5) was used to lyse and remove red cells from the cell suspension. To obtain bone-marrow-derived macrophages (MPs), monocytes were filtered through a 0.2 µm cell strainer and plated with high glucose DMEM supplemented with 10% fetal bovine serum (FBS, Gibco Life Technologies, #10500-064), Penicillin-Streptomycin (Life Technologies, #15140-122) and 20% L929 (Sigma-Aldrich, #85011425) conditioned medium as a source of macrophage colony stimulating factor (mCSF) for 6–8 d at 37 °C, 5% CO_2. Upon differentiation, MPs were detached with cold PBS and plated with fresh complete medium (with only 10% of L929 conditioned-medium) on PS or on different materials at a density of 27 000 cells cm^{-2}, unless differently specified, for the different time points needed.

Minocycline Preparation: Minocycline hydrochloride (Sigma-Aldrich, #M9511) was dissolved in DMEM at an initial concentration of 5×10^{-3} M, sonicated, and sterilized through a 0.2 µm filter. Minocycline solution was administered at final concentrations of 10×10^{-6} and 50×10^{-6} M. Because of its short half-life, the same amount of Minocycline was added after 12 h from the initial addition to the medium.

Immunocytochemistry and Immunohistochemistry: MPs were fixed with prewarmed 2% PFA and 2% sucrose in PBS for 5–10 min at RT and subsequently washed 3 times with PBS and conserved at 4 °C with 0.005% PBS sodium azide. Fixed cells were then incubated 30' at RT with 555 conjugated Phalloidin (Life Technologies, #A34055) diluted 1:100 in blocking solution [PBS + 10% Normal Goat Serum (NGS, PAA #B11-035)]. MPs were washed three times in 1X PBS and incubated for 3 min with 4′,6-diamidino-2-phenylindole (DAPI, 1:10.000 in 1X PBS) at RT in the dark. Finally, cells were washed twice with PBS, once with distilled water and mounted on glass microscope slides with mounting medium (DAKO, #S3023). Slides were stored at 4 or −20 °C.

Propidium iodide (PI) and Annexin V assay kit has been used to test cell viability. Cells were harvested, centrifuged at 1300 rpm for 3 min and the pellet carefully resuspended in 50 µL of staining buffer (10X Annexin V Binding buffer, eBioscience, #00-0055-56 diluted 1:10 in distilled water) containing Annexin V and PI (both diluted 1:50) and incubated for 20 min at RT in the dark. Cells were then diluted with additional 150 µL of buffer and analyzed with a flow cytometer.

Quantitative gene Expression Analysis: At the appropriate time point, MPs were collected from materials or PS using a cell scraper. For cells plated on materials (and their controls), total RNA was extracted using the miRCURY RNA Isolation Kit—Cell & Plant (Exiqon, #300110) accordingly to manufacturer instructions. Tetro cDNA Synthesis Kit (Bioline, #BIO-65043) was used to obtain cDNA starting from 100 µg of RNA. For bigger samples, cell pellets were resuspended with TRIzol reagent (Life Technologies, #15596-026) and total RNA was extracted following manufacturer description. 1000 ng of RNA were converted into cDNA using high capacity cDNA reverse transcription kit (Applied Biosystem, #4368813). For low-quantity samples, RTq-PCR was performed starting from 10 ng of cDNA using TaqMan Fast Universal PCR Master Mix (Life Technologies, #4352042) and read with a 7500 Fast Real Time PCR system machine (Applied Biosystem). The ΔΔCt method was used for quantification of gene expression. Expression levels were normalized to β-actin mRNA. All the experiments have been performed at least three times (three independent biological replicates).

Microscopy and Image Analysis: Fluorescent images were acquired using a Leica DMI 4000B inverted fluorescence microscope equipped with a Leica DFC3000 G camera or a Leica SPE DMI4000B scanning laser confocal microscope. For cell morphology analysis the long axis and short axis of each cell were manually traced and measured with Fiji software. The number of filopodia and the elongation factor were measured from 50 cells per experiment, selecting 5 isolated cells per field.

Heatmap of Materials' Properties: The heatmap was generated in *R* using the function heatmap.2 implemented in the gplots package. The expression data and the measurements of the materials' chemical–physical properties were scaled by subtracting to each value the mean value across all materials and dividing by the standard deviation of the mean. The row and column ordering as well as the dendrograms were obtained using the default hclust() function (complete method) on the distances computed by the dist() function (Euclidean distance).

Statistical analysis: Statistical analyses were performed using GraphPad Prism 5.0 software. One-Way analysis of variance (ANOVA) followed by Bonferroni's post hoc test correction was used for multiple group comparison, unless otherwise stated.

Acknowledgements

E.G. and M.D. contributed equally to this work. The authors thank Daniel Simon and Magnus Berggren from Linköping University, Sweden for discussing the experiments and providing us the PET samples. This research was supported by grants from: the EU 7th Framework Programme [FP7/2007–2013] under Grant Agreement No. 280772, "Implantable Organic Nanoelectronics (I-ONE-FP7)" project, the European Research Council (ERC) 2010-StG (RG 260511-SEM_SEM to S.P.); The Evelyn Trust (RG 69865 to S.P.), The Bascule Charitable Trust (RG 75149 to S.P.), The Great Britain Sakakawa Foundation to S.P.; MINECO (Spain) through project CSD2010-00024 and ERC-AdG-340177 to R.G.; and core support grant from the Wellcome Trust and MRC to the Wellcome Trust–Medical Research Council Cambridge Stem Cell Institute.

E.G., M.D., T.L., and S.P. designed the MP-on-materials experiments; E.G., M.D., and T.L. performed the experiments, acquired and analyzed the data; E.G., M.D., and S.P. interpreted the data. L.G.O. designed and provided PI and PEN substrates. A.C.D. and R.G. designed and analyzed the SCFS experiments. A.C.D. performed the SCFS and AFM measurements. G.F. and F.B. designed and made PLGA and PDMS films. G.F., S.C., M.B., and A.R. characterized the materials. F.B. integrated experimental results. E.G., M.D., R.G., S.P., and F.B. wrote the manuscript.

Received: February 4, 2017
Published online: March 30, 2017

[1] S. N. Jayasinghe, *Biomatter* **2013**, *3*, e25887.
[2] J. M. Anderson, A. Rodriguez, D. T. Chang, *Semin. Immunol.* **2008**, *20*, 86.
[3] D. T. Luttikhuizen, M. C. Harmsen, M. J. Van Luyn, *Tissue Eng.* **2006**, *12*, 1955.
[4] D. F. Williams, *Biomaterials* **2008**, *29*, 2941.
[5] E. M. Hetrick, H. L. Prichard, B. Klitzman, M. H. Schoenfisch, *Biomaterials* **2007**, *28*, 4571.
[6] P. Moshayedi, G. Ng, J. C. Kwok, G. S. Yeo, C. E. Bryant, J. W. Fawcett, K. Franze, J. Guck, *Biomaterials* **2014**, *35*, 3919.
[7] T. O. Collier, J. M. Anderson, W. G. Brodbeck, T. Barber, K. E. Healy, *J Biomed. Mater. Res., Part A* **2004**, *69*, 644.
[8] R. J. Schutte, L. Xie, B. Klitzman, W. M. Reichert, *Biomaterials* **2009**, *30*, 160.
[9] E. F. Irwin, K. Saha, M. Rosenbluth, L. J. Gamble, D. G. Castner, K. E. Healy, *J. Biomater. Sci., Polym. Ed.* **2008**, *19*, 1363.
[10] J. S. Hayes, E. M. Czekanska, R. G. Richards, *Adv. Biochem. Eng. Biotechnol.* **2012**, *126*, 1.
[11] J. Helenius, C. P. Heisenberg, H. E. Gaub, D. J. Muller, *J. Cell Sci.* **2008**, *121*, 1785.
[12] A. V. Taubenberger, D. W. Hutmacher, D. J. Muller, *Tissue Eng., Part B* **2014**, *20*, 40.
[13] M. Benoit, D. Gabriel, G. Gerisch, H. E. Gaub, *Nat. Cell Biol.* **2000**, *2*, 313.
[14] E. A. Evans, D. A. Calderwood, *Science* **2007**, *316*, 1148.
[15] I. R. Minev, P. Musienko, A. Hirsch, Q. Barraud, N. Wenger, E. M. Moraud, J. Gandar, M. Capogrosso, T. Milekovic, L. Asboth, R. F. Torres, N. Vachicouras, Q. Liu, N. Pavlova, S. Duis, A. Larmagnac, J. Voros, S. Micera, Z. Suo, G. Courtine, S. P. Lacour, *Science* **2015**, *347*, 159.
[16] A. Campana, T. Cramer, D. T. Simon, M. Berggren, F. Biscarini, *Adv. Mater.* **2014**, *26*, 3874.
[17] I. Tonazzini, E. Bystrenova, B. Chelli, P. Greco, P. Stoliar, A. Calo, A. Lazar, F. Borgatti, P. D'Angelo, C. Martini, F. Biscarini, *Biophys. J.* **2010**, *98*, 2804.
[18] F. Y. McWhorter, T. Wang, P. Nguyen, T. Chung, W. F. Liu, *Proc. Natl. Acad. Sci. USA* **2013**, *110*, 17253.
[19] P. K. Mattila, P. Lappalainen, *Nat. Rev. Mol. Cell Biol.* **2008**, *9*, 446.
[20] G. H. Ghassabeh, P. De Baetselier, L. Brys, W. Noël, J. A. Van Ginderachter, S. Meerschaut, A. Beschin, F. Brombacher, G. Raes, *Blood* **2006**, *108*, 575.
[21] K. A. Kigerl, J. C. Gensel, D. P. Ankeny, J. K. Alexander, D. J. Donnelly, P. G. Popovich, *J. Neurosci.* **2009**, *29*, 13435.
[22] R. Garcia, A. San Paulo, *Phys. Rev. B* **1999**, *60*, 4961.
[23] W. C. Oliver, G. M. Pharr, *J. Mater. Res.* **2004**, *19*, 3.
[24] R. Saha, W. D. Nix, *Acta Mater.* **2002**, *50*, 23.
[25] T. Ishimoto, T. Nakano, M. Yamamoto, Y. Tabata, *J. Mater. Sci.: Mater. Med.* **2011**, *22*, 969.
[26] M. Bianchi, M. Boi, M. Sartori, G. Giavaresi, N. Lopomo, M. Fini, A. Dediu, A. Tampieri, M. Marcacci, A. Russo, *J. Mater. Sci.: Mater. Med.* **2015**, *26*, 1.
[27] H. J. Butt, M. Jaschke, *Nanotechnology* **1995**, *6*, 1.
[28] V. A. Deshmukh, V. Tardif, C. A. Lyssiotis, C. C. Green, B. Kerman, H. J. Kim, K. Padmanabhan, J. G. Swoboda, I. Ahmad, T. Kondo, F. H. Gage, A. N. Theofilopoulos, B. R. Lawson, P. G. Schultz, L. L. Lairson, *Nature* **2013**, *502*, 327.